# *The effect of lipidation on the self-assembly of the gut-derived peptide hormone PYY3–36*

Article

Accepted Version

# The Effect of Lipidation on the Self-Assembly of the Gut Derived Peptide Hormone $PYY_{3-36}$

**Jessica A. Hutchinson, Samuel Burholt, Ian W. Hamley***

*Dept of Chemistry, University of Reading, Whiteknights, Reading RG6 6AD, U.K.*

**Anna-Karin Lundback, Shahid Uddin, Ana Gomes dos Santos**

*Medimmune, Granta Park, Cambridge CB21 6GH, U.K.*

**Mehedi Reza, Jani Seitsonen and Janne Ruokolainen**

*Department of Applied Physics, Aalto University, P.O. Box 15100, FI-00076 Aalto, Finland.*

**Abstract**

Lipidation is a powerful strategy to improve the stability in vivo of peptide drugs. Attachment of a lipid chain to a hydrophilic peptide leads to amphiphilicity and the potential for surfactant-like self-assembly. Here, the self-assembly and conformation of three lipidated derivatives of the gastrointestinal peptide hormone $PYY_{3-36}$ is examined using a comprehensive range of spectroscopic, scattering and electron microscopy methods and compared to those of the parent $PYY_{3-36}$ peptide. The peptides are lipidated at Ser( 11), Arg(17), or Arg(23) in the peptide, the former is within the β-turn domain (based on the published solution NMR structure), the latter are both within the α-helical domain . We show that it is possible to access a remarkable diversity of nanostructures ranging from micelles to nanotapes and fibrillar hydrogels by control of assembly conditions (concentration, pH and temperature). All of the lipopeptides self-assemble above a critical aggregation concentration (cac), determined through pyrene fluorescence probe measurements, and they all have predominantly α-helical secondary structure at their native pH. The pH and temperature dependence of the α-helical conformation were probed via circular dichroism

spectroscopy experiments. Lipidation was found to provide enhanced stability against changes in temperature and pH. The self-assembled structures were investigated using small-angle X-ray scattering (SAXS) and cryogenic transmission electron microscopy (cryo-TEM). Distinct differences in nanostructure were observed for lipidated and unlipidated peptides, also depending on the position of lipidation. Remarkably, micelles containing lipopeptides with $\alpha$-helical peptide conformation were observed. Gelation was observed at higher concentrations in certain pH intervals for the lipidated peptides, but not for unlipidated $PYY_{3-36}$. Thus lipidation, in addition to enhancing stability against pH and temperature variation, also provides a route to prepare PYY peptide hydrogels. These findings provide important insights into the control of $PYY_{3-36}$ conformation and aggregation by lipidation, relevant to the development of future therapeutics based on this peptide hormone, for example in treatments for obesity.

**Introduction**

Peptides are a very diverse class of molecules that play a crucial role in many in vivo processes, including their role as essential signalling molecules. A particular class of peptides are peptide hormones that have an effect on the endocrine system to control bodily functions.[5] Among peptide hormones, gastrointestinal hormones (gut hormones) such as Peptide YY (PYY) to control the functions of digestive organs are very important.[6-8] As a result, PYY and derivatives of it are being studied in the context of obesity treatment.

Peptides are rapidly broken down by enzymes in vivo and therefore are excreted from the body quickly. Lipidation of peptides can be used as a method to increase stability against environmental changes (pH, temperature, dilution etc),[9] and extend the half-life of peptide drugs circulating in the blood, thus increasing their therapeutic efficacy[10-12]. However, modification of peptides by adding a hydrophobic lipid chain could change the physiochemical properties such as; solubility, bioactivity, and/or conformation. It is also of great interest to study the effect of lipidation on possible formation of hydrogels by PYY peptides. Hydrogels may be useful as slow release delivery systems. As a result, it is important to understand what effects lipidation has on the overall structure and function of peptides as therapeutic agents.

Here, we study the influence that lipidation has on the self-assembly and conformation of the human gastrointestinal hormone $PYY_{3-36}$, and three lipidated derivatives that have palmitoyl chains covalently attached; one at position 11 (PYY11), another at position 17 (PYY17), and the other at position 23 (PYY23) (Figure 1c). The sequence of the 36-amino acid peptide, PYY is: Tyr-Pro-Ala-Lys-Pro-Glu-Ala-Pro-Gly-Glu-Asp-Ala-Ser-Pro-Glu-Glu-Leu-Ser-Arg-Tyr-Tyr-Ala-Ser-Leu-Arg-His-Tyr-Leu-Asn-Leu-Val-Thr-Arg-Gln-Arg-Try-$NH_2$ (Figure S5).[13] The lipid chain is linked to the peptide via a γ-glutamic acid spacer since this has been shown to enhance the potency (from a dose-response study of interaction with the receptor) of a lipidated peptide (GLP-1, glucagon-like peptide) compared to the unlipidated peptide and compared to other spacers.[14] We compare the self-assembly of lipidated

versus unlipidated $PYY_{3-36}$, and also how the position of lipidation affects the structure, using a range of physical characterisation techniques at varied pH and temperatures.

It is known that $PYY_{3-36}$ adopts a partially alpha-helical structure in aqueous solution.[4, 15] Residues from L(15) to T(30) are believed to lie in the $\alpha$-helical domain (Figure 1a). It is interesting to note that the helical wheel representation of the alpha helix of $PYY_{3-36}$ (Figure 1b) reveals a tendency for facial segregation of charged residues (bottom right) and uncharged residues (top left). Lipidation at residues 17, and 23 further enhances this effect (residue 11 is outside the $\alpha$-helical domain). The lipidated peptide structures are shown in Fig.1c. It may be noted that the helical wheel projection in Fig.1b suggests that homodimeric coiled coil formation is likely to occur.

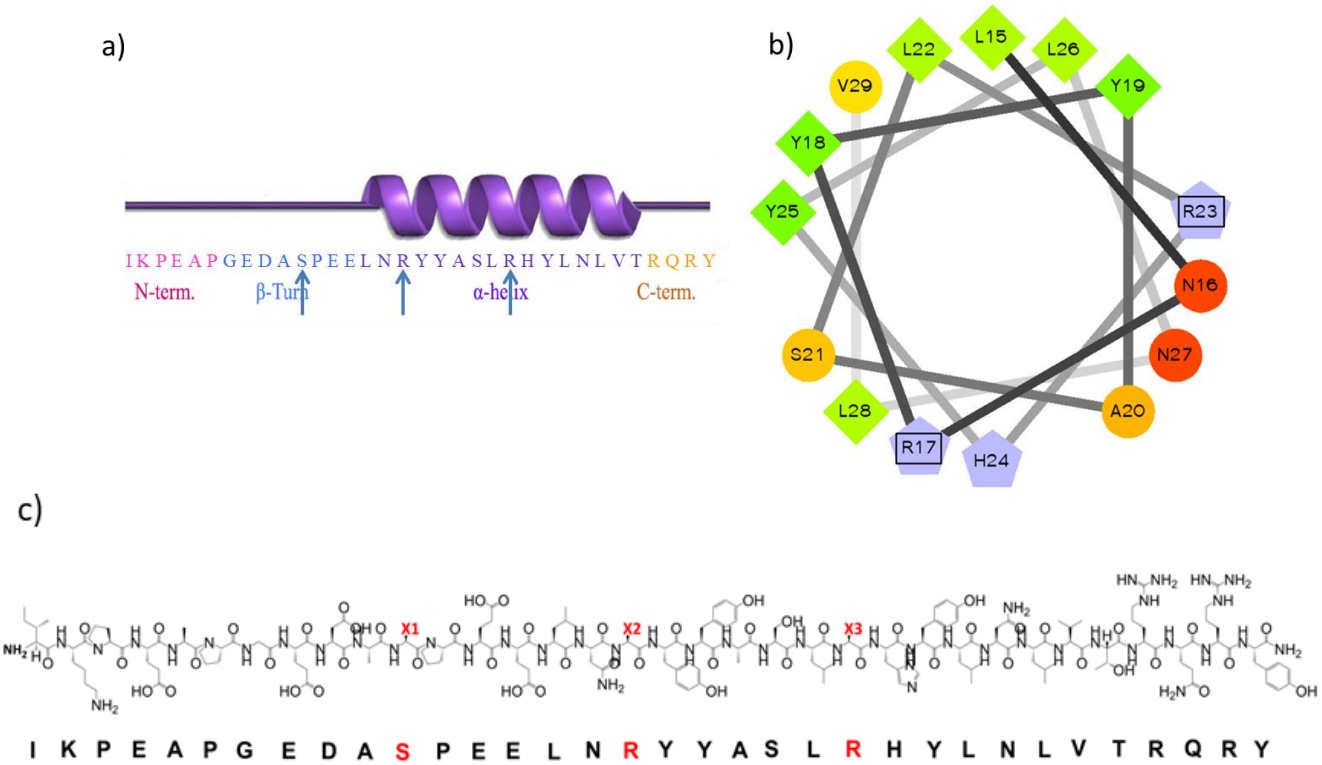


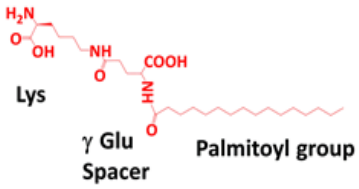


| | $X_1$ | $X_2$ | $X_3$ |
|---|---|---|---|
| **PYY11** | K | R | R |
| **PYY17** | S | K | R |
| **PYY23** | S | R | K |

**Figure 1:** a) Chemical structure of $PYY_{3-36}$ and the positions of lipidation (shown by arrows).[1] b) Helical wheel representation of $PYY_{3-36}$. The hydrophilic residues are represented as circles, hydrophobic residues as diamonds, and potentially positively charged as pentagons. Hydrophobicity is color coded: the most hydrophobic residue is green, and the amount of green decreases proportionally to the hydrophobicity, with zero hydrophobicity coded as yellow. The potentially charged residues are light blue. Hydrophilic residues are coded red with pure red being the most hydrophilic (uncharged) residue, and the amount of red decreasing proportionally to the hydrophilicity. The boxes indicate sites of lipidation with the residues indicated replaced with the lysine derivatives K(Glu Palm) with palmitoyl chains attached via a γ-glutamic acid linker.[2] c) Chemical structure of $PYY_{3-36}$ showing three lipidation positions (PYY11), 17 (PYY17), and 23 (PYY23). At each lipidation position, the amino acid present (Ser or Arg) is replaced with a lysine derivative in which the alkyl chain is attached via a γ- glutamic acid spacer.[3-4]

Peptide YY (PYY) is a gut hormone that belongs to the pancreatic polypeptide fold (PP-fold) family, characterised by a common tertiary structure, the PP-fold. Along with PYY, the pancreatic polypeptide (PP) and neuropeptide Y (NPY) also belong to this series of peptides.[16] All three peptides consist of a signalling peptide, followed by a 36 amino acid active peptide and a C-terminal amidation, which is very important for the binding of agonists to the Y receptors.[17] PP and NPY have amino-terminal tyrosine residues, and PYY has a tyrosine residue at the C-terminal and at the N-terminal, hence the name name PYY.[18]

This family of peptides mediate their effects through the NPY receptors Y1, Y2, Y4, and Y5.[19] The Y-receptors belong to the G-protein-coupled receptor family, and they mediate a wide variety of physiological effects such as regulation of blood pressure, anxiety, memory retention, hormone release, and food intake.[20]

The L-cells in the gastrointestinal tract release PYY following food intake, and there are two main endogenous forms: $PYY_{1-36}$ and $PYY_{3-36}$. The 36 amino acid peptide, $PYY_{1-36}$ is rapidly hydrolysed to the 34 amino acid peptide, $PYY_{3-36}$ by the peptidase enzyme DPP4 which removes the first two amino acids; tyrosine and proline at the N-terminus.[21] This alters the receptor selectivity and as a result $PYY_{3-36}$ has a high selectivity for the Y2-receptor, compared to $PYY_{1-36}$ which has selectivity for the Y1, Y2, and Y5 receptors.[22] The Y1 receptor is believed to require both the C-terminus and N-terminus for recognition, whereas The Y2 receptor only requires the C-terminus. It is understood that the Y2 receptor has a smaller receptor binding site,[5] and this could explain the reduced affinity for $PYY_{3-36}$ on any Y receptor other than Y2.[3] Other studies replacing the amide bonds with ester bonds also confirm that the C-terminus is important in binding and activation.[23]

The Y2-receptors are strongly expressed in the epithelia of the visceral tissues, including the colon and the kidney, and have been associated with reduced food intake via the vagal inhibitory loop,[17] and also gastric emptying.[22] The Y2-receptor is therefore considered a target for the treatment of obesity and type 2 diabetes. There is an urgent unmet need for treatments for obesity which is of

increasing relevance, and peptide drugs derived from peptide hormones are attracting increasing interest. Peptide-derived drugs may have advantages compared to synthetic small molecule drugs in; reduced toxicity, higher selectivity, and greater predictability in their in-vivo behaviour.[11] In contrast however, the use of peptides and proteins as therapeutic agents has its drawbacks due to their rapid degradation, excretion, and poor water solubility. The application of $PYY_{3-36}$ as an anti-obesity drug is a very interesting avenue of research, but is limited by its short half-life of around 9 minutes.[18]

One of the main reasons for the short half-life of peptides is their rapid clearance from circulation via several mechanisms, which makes it difficult to use them as drugs. Mechanisms involved in their clearance include peripheral blood-mediated elimination by proteolysis, renal and hepatic elimination, and also receptor-mediated endocytosis.[24] A dominant factor for such rapid clearance is molecular weight. Molecules that have a low molecular weight (< 40-50 kDa) are rapidly cleared by renal filtration via the glomerular filtration barrier (GBM) into the urine. As a result of this, increasing the size of a peptide drug is a good starting point to improve half-life.[25]

Methods to increase molecular weight include lipidation and PEGylation. Lipidation is the attachment of one or more fatty acid chains to the peptide, and as an additional benefit it protects against proteolytic attack, by allowing the peptide to non-covalently bind to plasma proteins. PEGylation is the covalent attachment of polyethylene glycol (PEG) chains to the peptide which also has this effect, whilst providing a higher solubility in water. Furthermore, allergic reactions are reduced, but not eliminated.[11, 26-27] Unfortunately however, even though covalently attaching PEG prolongs half-life in vivo, it can also lead to loss of biological activity.[28] A study on lipidation and PEGylation on the GLP-1 peptide was carried out and the results showed that lipidation had no significant effect on peptide activity in vitro,[29] whereas PEGylation did, especially when the PEG is attached to internal amino acids of the peptide e.g. positions 20 and 21. The reduction in activity from PEGylation compared to lipidation is due to the loss of receptor affinity. It is suggested that this

is because of its high molecular weight which causes steric hindrance.[30-31] In another study, PEGylation of human pancreatic peptide (hPP) has been shown to lead to reduced food intake in a mouse model. PEGylation was found to protect against enzymatic degradation, enhancing bioavailability.[32]

Lipidation as a method of extending half-life is becoming more widely used in the development of peptide drugs.[10-12] Lipidation is similar to PEGylation whereby both increase the hydrodynamic radius to reduce renal filtration. The lipid chain itself however, is too small to mediate this effect alone, and so it does it by non-covalently binding to circulating serum albumin, to protect the whole complex from proteolytic cleavage.[10]

An example of a lipidated peptide drug is Liraglutide, which is the highest selling diabetic drug currently on the market. It is a GLP-1 agonist that requires once a day administration. Liraglutide incorporates a palmitoyl lipid chain at position 26 to prolong plasma circulation and bioactivity.[5] The mediated effects occur by the palmitoyl chain non-covalently binding to serum albumin as previously mentioned. This prevents proteolytic attack by DPP4 due to steric hindrance, and also rapid renal clearance via the GBM because of the increased molecular weight. As a result, this provides a very promising avenue of research, because if similar results can be achieved with $PYY_{3-36}$, then a new peptide drug could be potentially introduced to the market to treat obesity and type II diabetes.

Here, we investigate the influence of lipidation on the conformational stability of $PYY_{3-36}$ to changes in pH and temperature. We also probe the self-assembled nanostructure as a function of pH and temperature using a powerful combination of fluorescence assays, circular dichroism (CD) spectroscopy, small-angle x-ray scattering (SAXS), X-ray diffraction (XRD), cryogenic transmission electron microscopy (cryo-TEM), and transmission electron microscopy (TEM), to compare the three lipidated peptides to the unmodified peptide. In addition, we have found conditions where PYY11, PYY17 and PYY23 form hydrogels, which are not observed for the unlipidated peptide.

**Results**

Three lipidated derivatives of $PYY_{3-36}$ were characterised to determine whether lipidation has an effect on peptide conformation and/or if it led to self-assembly due to the induced amphiphilicity caused by lipidation. Palmitoyl chains were covalently attached to the peptides, by substitution at position 11 (PYY11), 17 (PYY17), or at position 23 (PYY23) of γ-L-glutamoyl($N^{\alpha}$-hexdecanoyl) lysine residues as shown in Figure 1c. The unlipidated peptide was also characterised for comparison (Figure S2).

The presence of a possible critical aggregation concentration (cac) for possible self-assembly was investigated using pyrene as a fluorescent probe. Pyrene is a fluorophore that is sensitive to the local hydrophobic environment,[33] and it has been used a number of times previously to determine the cac of peptides and peptide amphiphile molecules.[34-35] The cac of the peptides were calculated by measuring the fluorescence intensity of the $I_1$ (λ = 373 nm) peak, corresponding to the first vibronic band of pyrene. The dependence of the intensity $I_1$ (373 nm) with the peptide concentration is shown in Figure 2. The fluorescence intensity shows breaks at 0.013 wt%, 0.015 wt%, and 0.0091 wt% (± 0.005 wt %) for PYY11, PYY17, and PYY23 respectively, at their native pH in ultrapure water (pH 4). The native pH is defined as the pH of the solution when the peptide is dissolved in ultrapure water. These breaks are due to the change in the local hydrophobic environment of pyrene, indicating these as the cac values. Above the cac concentration, pyrene becomes incorporated within the hydrophobic environment of the aggregated peptide core, and this is what causes the distinct increase in the intensity. The same method was used to probe the pH dependence of the cac. Plots $I_1$ / $I_3$ [I (373 nm)/I (383 nm)] corresponding to the ratio of the intensities of the first to third vibronic bands of pyrene is shown in the SI (Figures S3-S5), but the cac was not well defined for PYY11 or for PYY23 at pH 2 using this ratio. However from previous studies reported, using other fluorescent probes to compare to pyrene, the concentration dependence of $I_1$ provides a reliable

assay for cac values.[34, 36] Results indicate that the cac values are lower for the peptide solutions at native pH compared to pH 2 and pH 8.

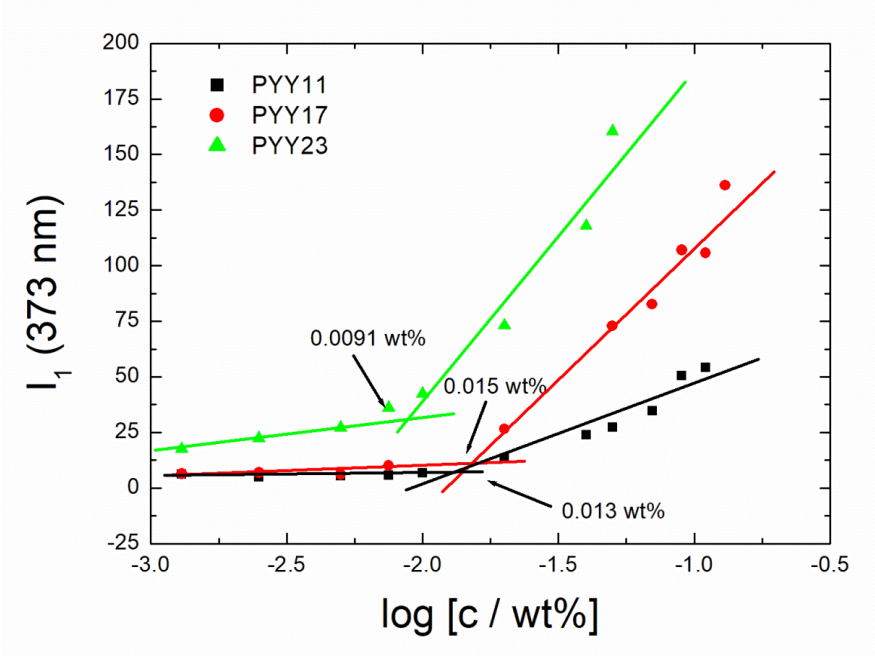


**Figure 2:** Concentration dependence of pyrene fluorescence $I_1$ (373 nm) of PYY11, PYY17, and PYY23 at native pH (pH 4). The intersections of the lines defines the critical aggregation concentration (cac).

Titrations were carried out to determine the isoelectric point (pI) of each peptide because calculated values were significantly different from the point at which precipitation was observed. At around pH 6 was the pH of precipitation, this being tentatively associated with experimental pI. Experiments were carried out using 2 wt% peptide solutions and the starting pH was pH 10 following the addition of NaOH. The pH was plotted as a function of added volumes of HCl, where HCl was added dropwise. The plot indicates that the pH shows an initial sharp decrease with a plateau at around pH 5, close to the pH at which precipitation occurs. This is associated with an effective pI (Fig. S6). The exact isoelectric point of each peptide was not able to be measured from the titration graph due to the range of pKa values of the residues within the peptide sequences. The Henderson-Hasselbach equation was used to calculate the charge versus pH, and the isoelectric points were calculated (where z = 0) to be pH 10.07 for $PYY_{3\text{-}36}$ and PYY11, and pH 9.1 for PYY17 and PYY23 respectively.

Only two values were calculated because PYY3-36/PYY11 and PYY17/23 have the same pKa values of residues, and so they have similar curves as shown in both the experimental titration graph, and also the calculated charge versus pH graph (SI Fig. 6 and 7).

It is well known that the pKa of residues in proteins can be very substantially shifted from ideal values for isolated residues due to sequestration within hydrophobic compartments and/or the effect of electrostatic interactions between close charged residues.[37-38] In less polar environments (for example in hydrophobic domains of self-assembled structures) the pKa values for acidic residues will be higher than expected, whilst for basic groups pKa values will be lower than normal.[38] In addition, self-assembly of peptides can also cause very significant (more than 6 pH units) apparent pKa shifts as exemplified by measurements on hydrophobically-modified peptides.[39]

Zeta potential measurements were carried out at pH 2 and 4 to determine particle charge on the peptides. All values were positive, indicating that the peptides all have positive a charge under these conditions (Table S1).

The secondary structures of $PYY_{3-36}$, PYY11, PYY17, and PYY23 were examined using circular dichroism (CD) spectroscopy well above the cac values. Temperature ramp experiments were carried out at pH 2, 4, 6 and 8 from 20-70 $^{o}$C. Figure 3 shows CD spectra of all peptides in the pH range 2-8 at 20 $^{o}$C and SI Fig. S8 shows the spectra at 70 $^{o}$C. The spectra at 20 $^{o}$C for all samples studied show two minima near 222 nm and 208 nm, and these features are typical of $\alpha$-helical secondary structure, and are consistent with coiled coil formation.[40-42]

The $\alpha$-helix content was calculated based on an extrapolated value for the molar ellipticity, reported for an infinite length 100% helical peptide, where $[\Theta]$ = -37,400 deg cm$^2$ dmol$^{-1}$. [43-44] The results (Figure 4) indicate that the position of lipidation does not appear to affect the secondary structure, apart from PYY11 at pH 8 where the $\alpha$-helix content is significantly decreased. The calculated $\alpha$-helical content of the peptides is summarized in Table 1. Apart from PYY11 at pH 8, each lipidated

peptide shows a reduced dependence of α-helix content on pH and temperature compared to $PYY_{3-36}$ (Figure 4 and Table 1). This important result shows that lipidation enhances the stability of the natural α-helical domain to changes in pH and temperature.

When increasing the temperature to 70 $^{0}$C, there appears to be a transition into β-sheet above 50 $^{o}$C for PYY17 and PYY23 at pH 8, with a minimum near 217 nm, characteristic of β-sheet secondary structures (Fig. S8c).[40-42] This transition could be related to the lower isoelectric point for PYY17 and PYY23 compared to PYY11 and $PYY_{3-36}$. At pH 8, PYY17 and PYY23 are expected to have a charge of +1, meaning that there are only weak interactions to overcome in order to aggregate, and that hydrogen bonding can more readily overcome the electrostatic interactions to form a β-sheet structure.[45] Interestingly, PYY11 does not undergo this transition, which suggests that the position of lipidation is causing a difference in the stability of the secondary structures. It seems that lipidating the peptide outside of the α-helical region of the molecule, reduces the tendency for β-sheet formation at high pH. $PYY_{3-36}$ does not undergo this transition either, suggesting that the increased amphiphilicity of the lipidated peptides PYY17 and PYY23 influences the secondary structure, at higher pH.

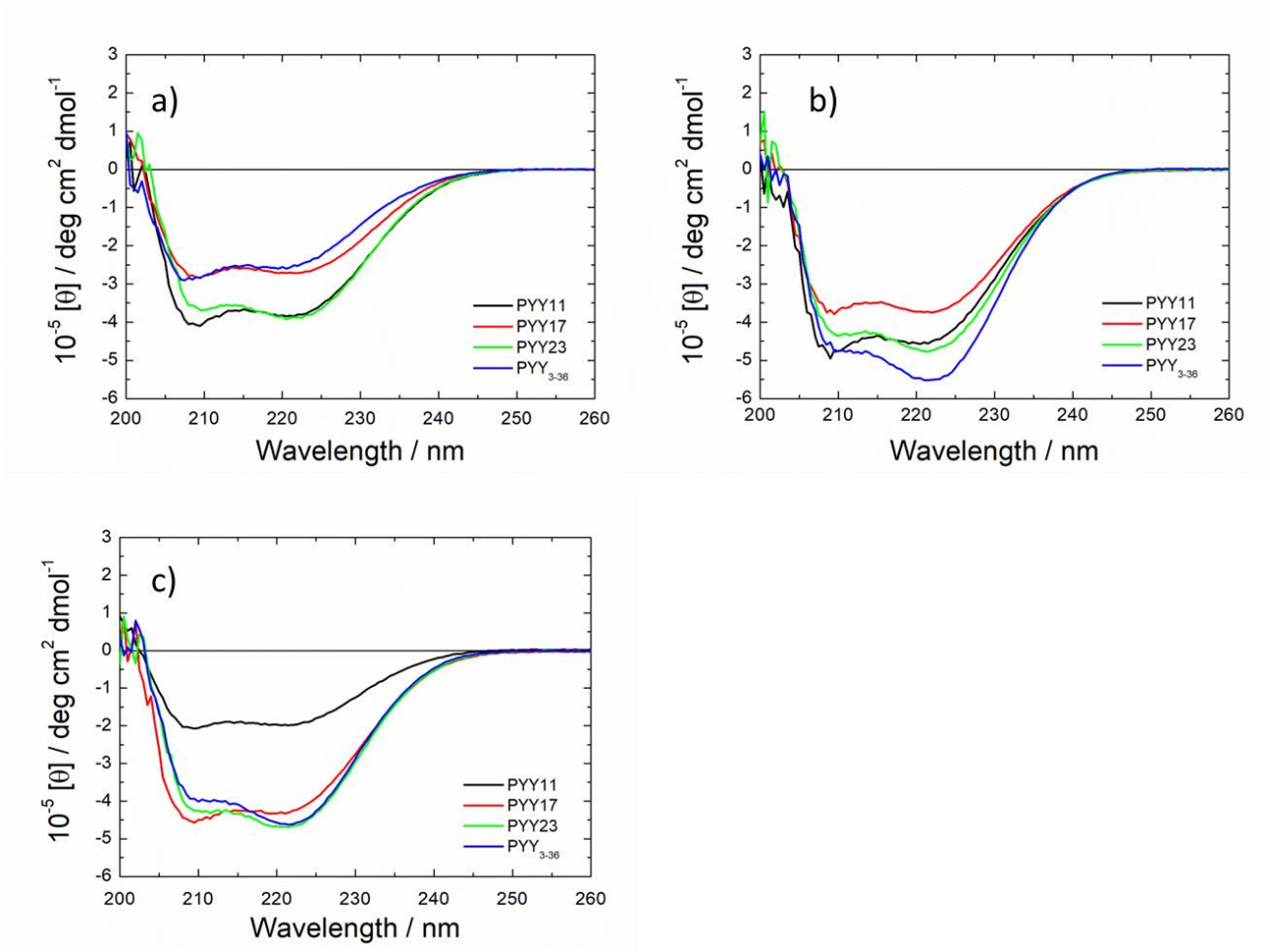


**Figure 3:** CD spectra of 0.5 wt% solutions of PYY11, PYY17, PYY23, and PYY$_{3-36}$ at 20 °C. a) pH 2, b) native pH (pH 4 for lipidated peptides, and pH 6 for unlipidated peptide), c) pH 8.

The lower stability of PYY$_{3-36}$ to temperature changes is also shown by the significant decrease in molar ellipticity upon heating (Figure 4). The full set of temperature-dependent CD data is shown in Figures S9-S12. Figures S9c, S11c, and S12c show CD spectra at pH 6, however it should be noted that at this pH the peptide solutions formed precipitates, reducing the molar ellipticity values. The

results in Figure 4 show that PYY23 has the highest α-helical content out of all three lipidated peptides studied throughout the whole pH and temperature range. This is the peptide which is lipidated in the core of the α-helical domain (Figure 1a).

**Table 1:** Calculated $\alpha$-helix content of $PYY_{3-36}$, PYY11, PYY17, and PYY23 at pH 2, native pH in ultrapure water (pH 4 for lipidated and pH 6 for unlipidated peptide), and pH 8, at 20 °C.

| Helix content (%) at 20 °C | pH 2 | pH 4<br><br>(native pH of peptide when dissolved in ultrapure water) | pH 8 |
|---|---|---|---|
| $PYY_{3-36}$ | 19.9 | 43.3 | 36.3 |
| PYY11 | 29.9 | 35.3 | 15.5 |
| PYY17 | 21.4 | 35.0 | 33.5 |
| PYY23 | 30.5 | 37.3 | 36.6 |

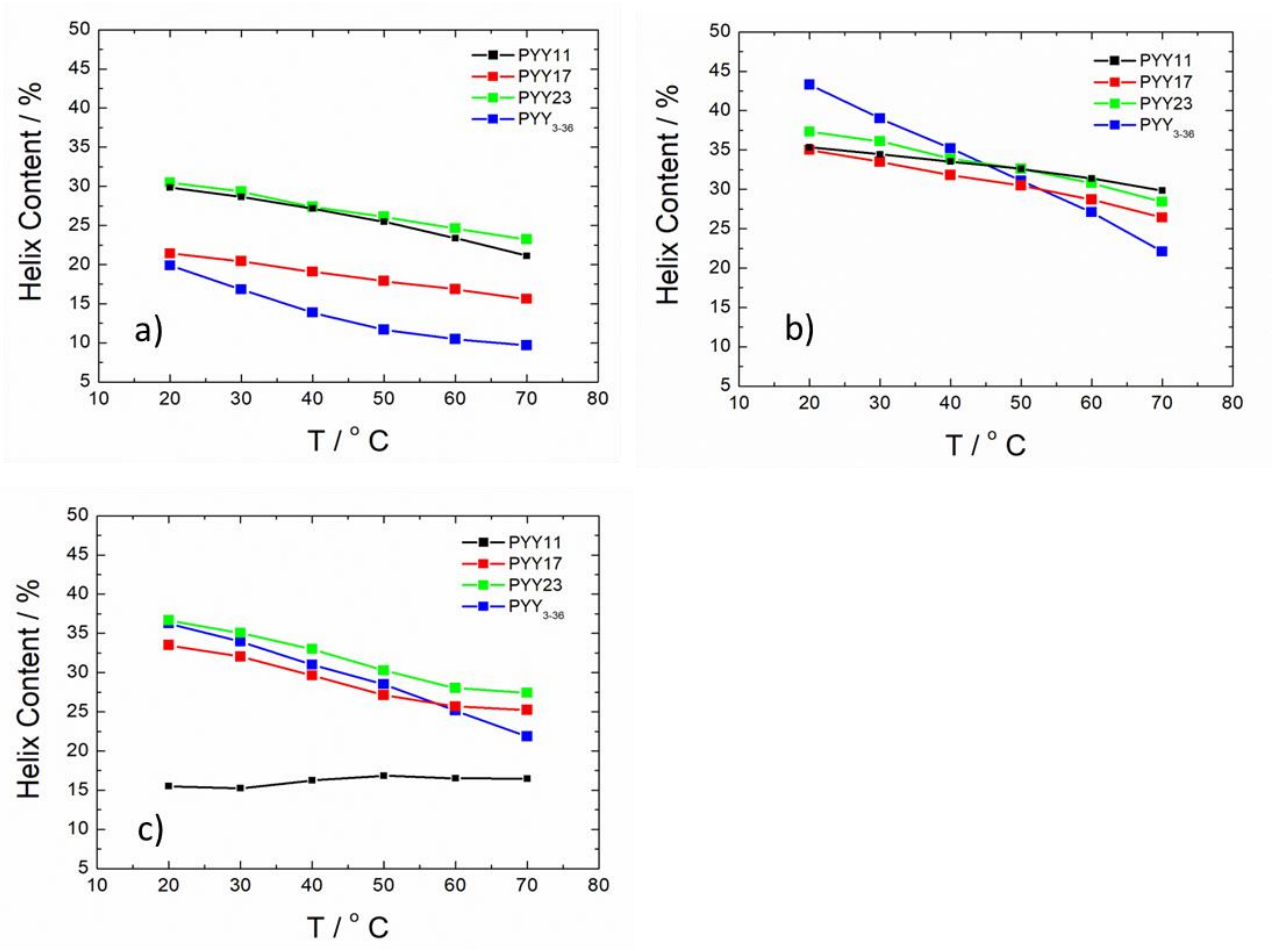


**Figure 4:** Calculated α-helix content of $PYY_{3-36}$, PYY11, PYY17, and PYY23 at; a) pH 2, b) the native pH of the peptide (pH 4 for lipidated peptides and pH 6 for native $PYY_{3-36}$, and c) pH 8, 20-70 °C.

The morphology of aggregates of the lipidated peptides and $PYY_{3-36}$ itself was examined by SAXS and cryo-TEM. Cryo-TEM avoids the need to dry or stain the sample, by vitrifying the solution, allowing the self-assembled structures to be seen. Images of all three lipidated peptides at pH 2 and 8 are shown in Figure 5. The images indicate the presence of long entangled fibers with some globular objects, with variable lengths of several hundred nanometres for PYY11 at pH 8, PYY17 at pH 2-8, and PYY23 at pH 4 and pH 8. Although the fibril length cannot be accurately determined at these magnifications, the fibril radius is measured as; 8.0 nm (± 1.6 nm) at pH 4, and 2.9 nm (± 0.5 nm)at pH 8 for PYY17, and 8.2 nm (± 1.6 nm), and 2.7 nm (± 0.5 nm) at pH 4 and 8 respectively for PYY23. Accurate radius values of PYY11 fibrils could not be measured due to the entangled nature of the structures, making it too difficult. However the radius was observed to be approximately less than

10 nm. Images of PYY11 at pH 2 and 4, and PYY23 at pH 2 show the appearance of micelles with an average radius of 4.8 nm (± 0.7 nm) and 3.7 nm (± 0.8 nm) for PYY11 and 23 respectively (Figure 5). It is also very interesting to see that the position of lipidation affects the aggregated structure at pH 2, where PYY17 forms fibers, and PYY11 and PYY23 form micelles. This is presumably due to enhanced electrostatic interactions between charged residues in PYY11 and PYY23. Additional cryo-TEM images are included in Figures S13-16. The native peptide forms twisted nanotapes (Figure. S16); it is clear from this type of nanostructure that lipidation causes a change in aggregation, especially at low pH.

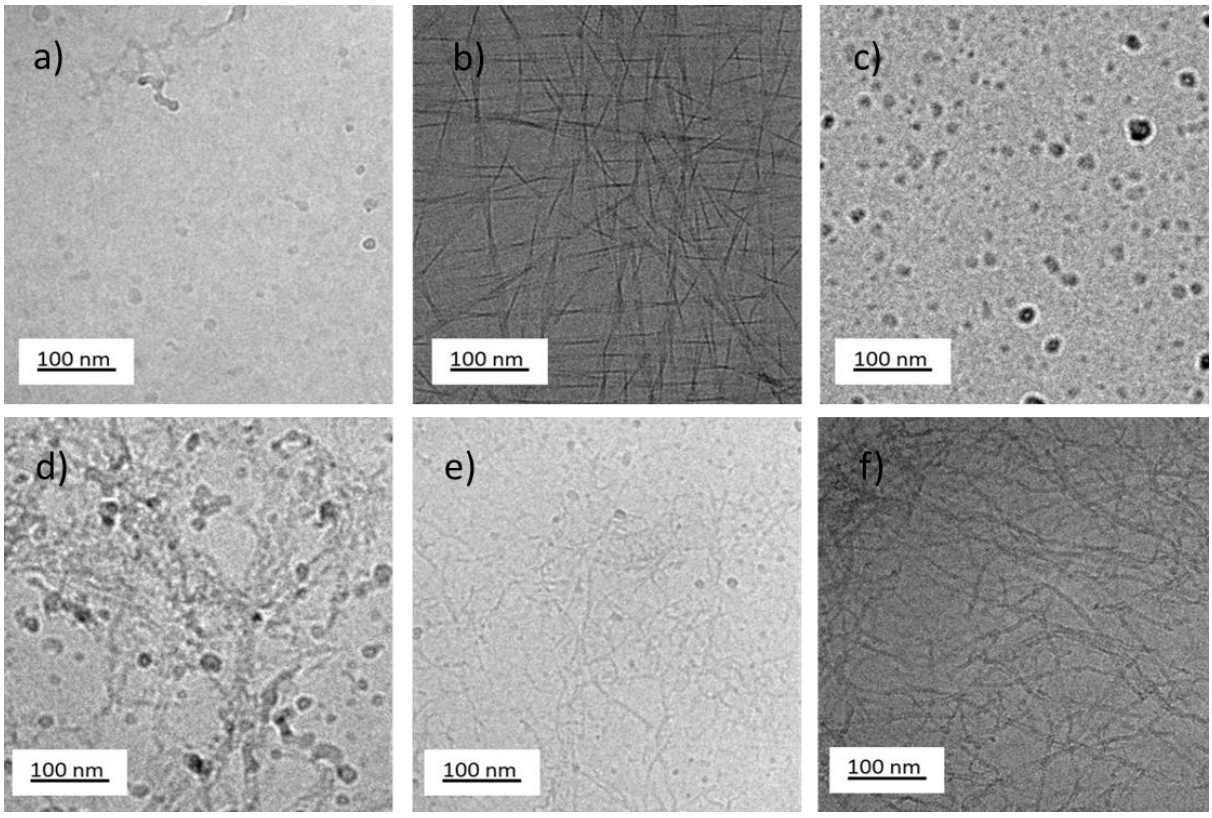


**Figure 5:** Cryo-TEM images of PYY11, PYY17, and PYY23. a) PYY11 pH 2, b) PYY17 pH 2, c) PYY23 pH 1.90, d) PYY11 pH 8, e) PYY17 pH 8.22, f) PYY23 pH 8.

Cryo-TEM was complimented with SAXS, which provides accurate dimensions and internal structures of the nanostructures. The SAXS intensity profiles for PYY11, 17 and 23 are shown in Figure 6. The data for $PYY_{3-36}$ is shown in Figure S17. The scattering data can be fitted to a spherical shell form factor for PYY11 at pH 2 and 4 and for PYY23 at pH 2. A long cylindrical shell form factor was used to

fit the remaining data. SAXS data of the native peptide, $PYY_{3-36}$ was fitted to a generalized Gaussian coil at pH 2 and 6. Although cryo-TEM images show a population of twisted nanotapes the SAXS profiles are dominated by monomers. The data at pH 8 was fitted to a bilayer Gaussian form factor which is used to represent nanotape structures formed by stacked β-sheet layers.[46-48] Cryo-TEM images of $PYY_{3-36}$ at pH 8 showed clusters of aggregates but the SAXS data (Fig. S20) indicated the presence of sheets. This gives a vast contrast to the lipidated peptides, indicating that lipidation significantly changes self-assembly throughout the whole pH range (pH 2-8). The fitted parameters are listed in SI Tables S4 and S5. The fittings were carried out using the software SASfit.[49]

A notable observation when comparing SAXS data of the lipidated peptides across the whole pH range is the difference in radius (R) and shell thickness (DR) values (Fig. S21). Changing the pH of PYY17 away from its native pH caused the radius to decrease, whereas for PYY23 the opposite occurred, whereby increasing the pH caused the radius value to increase. As the pH was raised from 2-8, the shell thickness for both PYY17 and 23 also increased. For PYY17, the shell thickness increased from 0.113 nm to 0.271 nm when increasing the pH from 2-8.

Figure 7 summarizes our observations on the self-assembly and conformation of the three lipidated peptides; PYY11, PYY17 and PYY23 at different pH values and relates it to the expected charges on the residues at different pH values (with the caveat mentioned above that the residue pKa values may be significantly changed by aggregation). It is that the lipopeptides retain α-helical structure even within micelles. Our results provide evidence for unique conformationally ordered lipopeptide micelles. The schematic in Fig.7 does not represent the actual association number, which is estimated to be ~7 based on the micelle radii from SAXS fits (SI Tables S4 and S5) along with the estimated molecular volume of PYY3-36 (4901 $Å^3$).

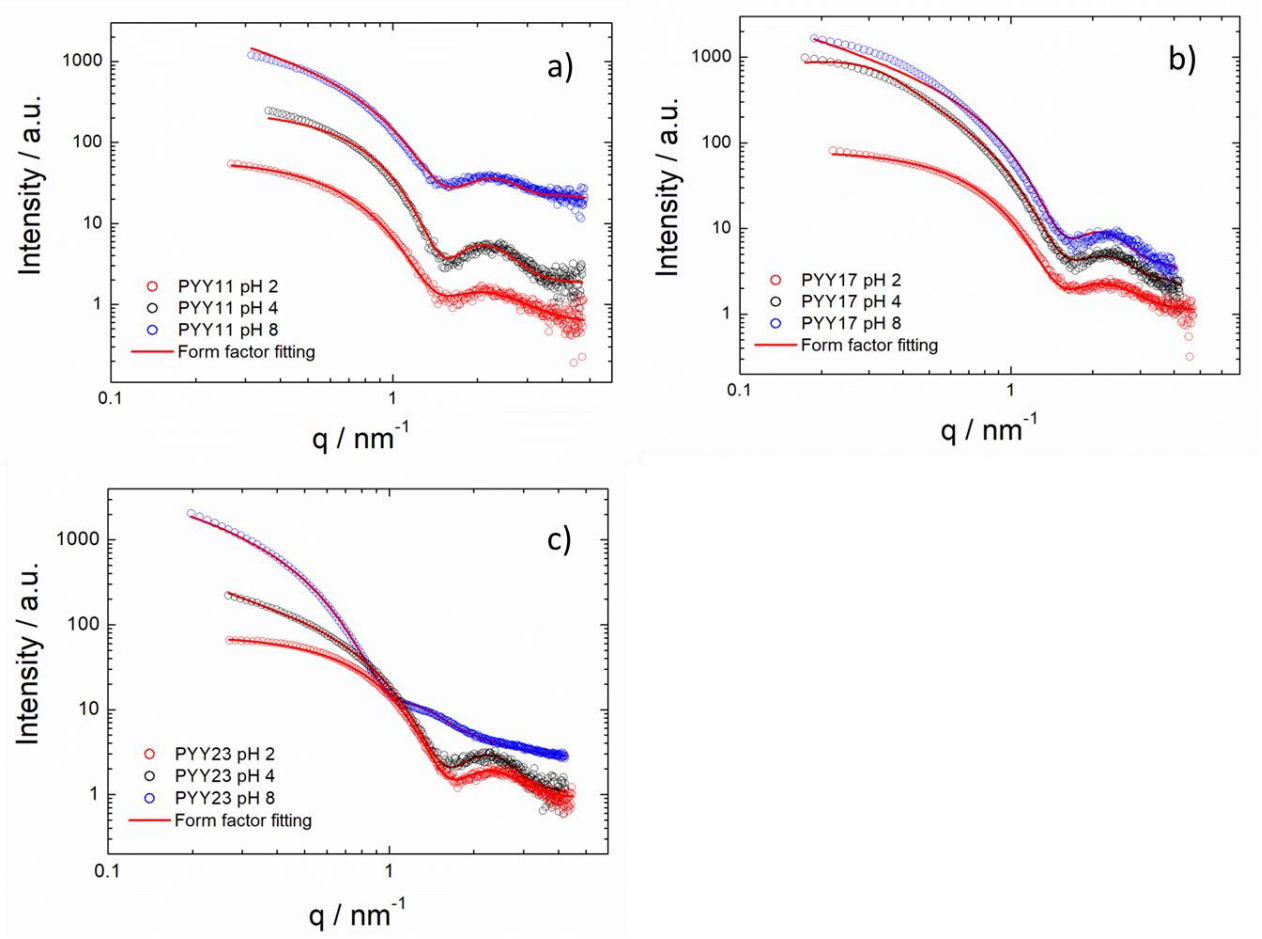


**Figure 6:** SAXS intensity profiles. a) PYY11, b) PYY17, c) PYY23 at pH 2-8. All samples were at 0.5 wt% and 20 $^{o}$C. PYY11 data was fit to a spherical shell form factor at pH 2 and 4, and a long cylindrical shell form factor at pH 8. PYY17 data was fit to a long cylindrical shell form factor for all pH values. PYY23 was fit to a spherical shell form factor at pH 2 and a long cylindrical shell form factor at pH 4 and 8.

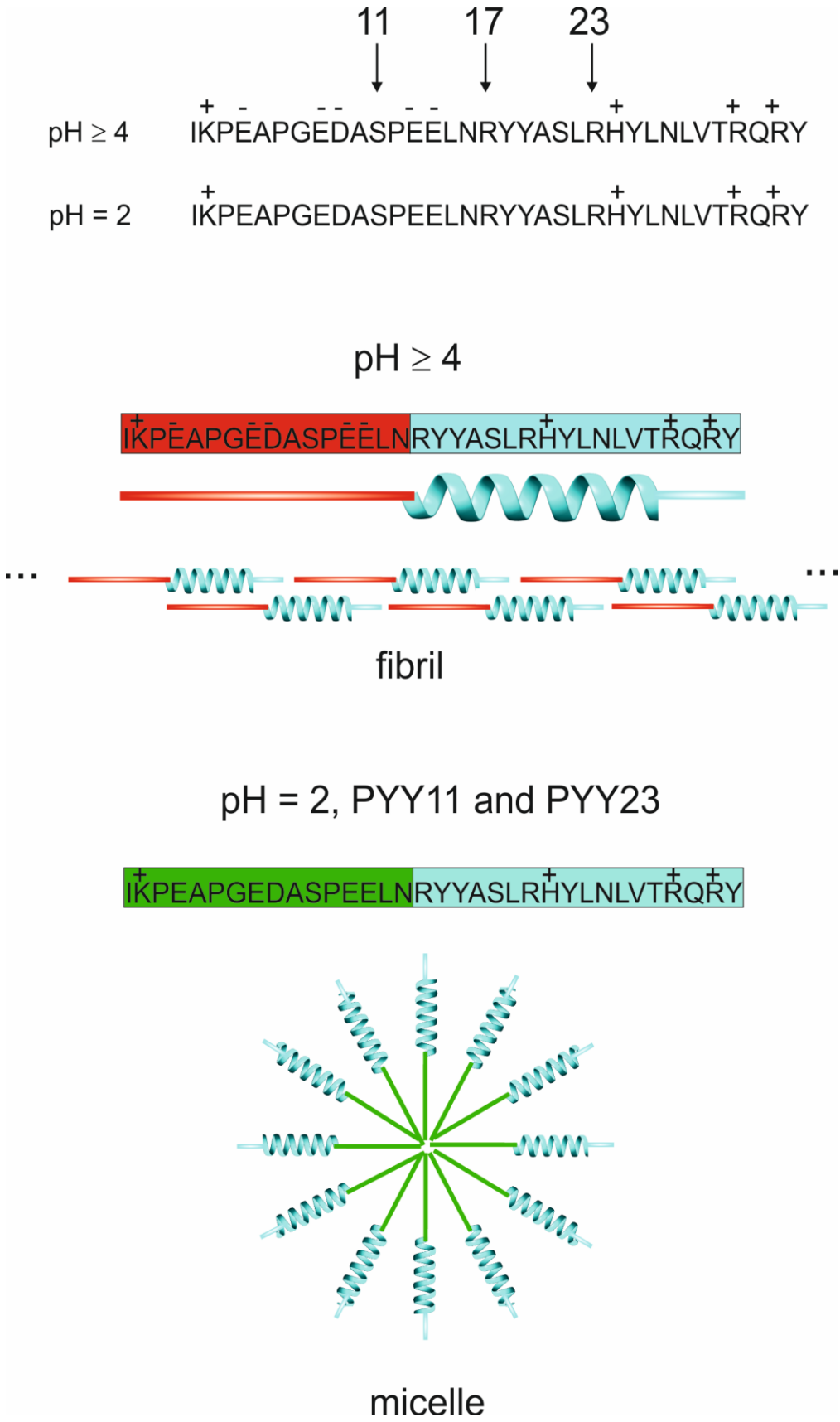


**Figure 7:** Proposed model to show how the charges on particular amino acid residues can influence the self-assembly under different pH conditions. The arrows indicate the sites of K(Glu $P_c$Palm) lipidation.

**Hydrogel Studies**

The formation of hydrogels by lipidated peptides is relatively rarely observed. Among a handful of studies, gel formation has been reported for β-sheet nanofiber-forming lipidated peptides when the fibrils form a sample-spanning network under suitable conditions of pH,[50-56] or by addition of salts[52, 54, 57-58] or small molecule compounds.[59] Castelletto *et al*. reported the observation of hydrogels for three lipidated peptides containing a lumican peptide sequence and three different lipid chain lengths ($C_{12}$-, $C_{14}$- and $C_{16}$-) by pH adjustment.[60] Uniquely, these hydrogels are based on nanotape structures rather than cylindrical fibrils. A recent report shows that it is possible to create hydrogels from α-helical peptides by careful design of the sequence.[61] Coiled coil peptides can be designed to co-assemble into dimers with complementary sticky ends that can then associate into fibrils. In the context of therapeutics, hydrogel formulations of peptides are of interest for slow-release formulations. We therefore sought to examine whether it is possible to create hydrogels from the lipidated peptides or $PYY_{3-36}$ itself.

Cryo-TEM and SAXS of the lipidated peptides showed the presence of extended fibrils in the pH range 4-8 for PYY17 and 23, and pH 6-8 for PYY11. In this case a simple pH change and evaporation method was used to form the hydrogels. CD and fibre XRD were performed to investigate conformation, along with SAXS and TEM to probe morphology. Polarized optical microscopy (POM) was also used to observe green birefringence from the formation of amyloid fibrils. The concentration of peptide in the gels was measured in the range 1.6-2.4 wt% using a nanodrop instrument.

Gelation was confirmed using the inverted vial method. Samples where gelation did not occur are shown to allow for comparison. The formation of gels using the unmodified peptide was also attempted; however gelation did not occur over the range of pH conditions examined. Representative images are shown in the SI (Figures S19 and S20).

Samples with a wide range of pH values were prepared to investigate the effect that pH had on gelation. Table 2 summarises the pH values at which gels were formed for all three lipidated peptides. It was noted that all lipidated peptides at pH 8 transformed readily into gels and this pH was the most well controlled for formation, with other pH values needing longer time periods, up to 10 hours to form. We did not observe hydrogel formation by $PYY_{3-36}$ itself under the conditions of pH and concentration examined.

There is no gel formation until pH 7-8 for PYY11 and also between pH 4 and 6 for both PYY17 and PYY23. At around pH 6, the samples in solution formed precipitates, suggesting that this pH is close to the PI of the peptides as discussed above, and this might have had an effect on gelation. The reason for gelation not occurring between pH 4 and 6 may be due to increased charge on the peptides in this pH range due to the pKa values of the charged residues. This is very hard to quantify because the pKa in peptides can shift upon aggregation.[62-63] Our results show that it is possible to produce hydrogels by lipidating $PYY_{3-36}$ and adjusting the pH to be sufficiently high or low.

**Table 2:** Summary of conditions for gel formation. Gelation did not occur with the unlipdated peptide.

| Successful pH values for gel formation (± 0.01) | | |
|---|---|---|
| **PYY11** | **PYY17** | **PYY23** |
| pH 8.47 | pH 3.80 | pH 3.19 |
| pH 8.76 | pH 7.35 | pH 6.09 |
| | pH 7.77 | pH 6.11 |
| | pH 8.67 | pH 6.56 |
| | pH 8.88 | pH 7.16 |
| | | pH 8.57 |
| No gels formed from un-lipidated $PYY_{3-36}$ | | |

CD studies were performed on the gels at pH 6-8, to probe the secondary structure. Results at pH 8 are shown in Figure 8a and they indicate that the gels adopt a β-sheet secondary structure the spectra showing a minimum near 217 nm, .[40-42] compared to the peptides in solution which showed

an α- helical structure. An interesting point to note is that at pH 6, PYY17 did not form a gel, but the CD data still shows β-sheet structure with a minimum at 217 nm (Figure S21). As a result, it is suggested that the mechanism behind gelation is a combination of pH change, and a thermal transition from α-helix to β-sheet.

The thermal transition from α-helix to β-sheet of PYY11 was examined using CD at pH 8 since this was the pH at which all lipidated peptides formed the strongest gels (Figure S22). The experiment was carried out using a 2 wt% peptide solution and the pH was changed using NaOH (0.5M) and HCl (0.5 M). The sample was heated in a water bath at 60 °C and measurements were taken every 20 minutes until the transition occurred. The results show that the transition started to occur at 60 minutes and by the 80 minute measurement the structure was fully β-sheet with a minimum at 218 nm.

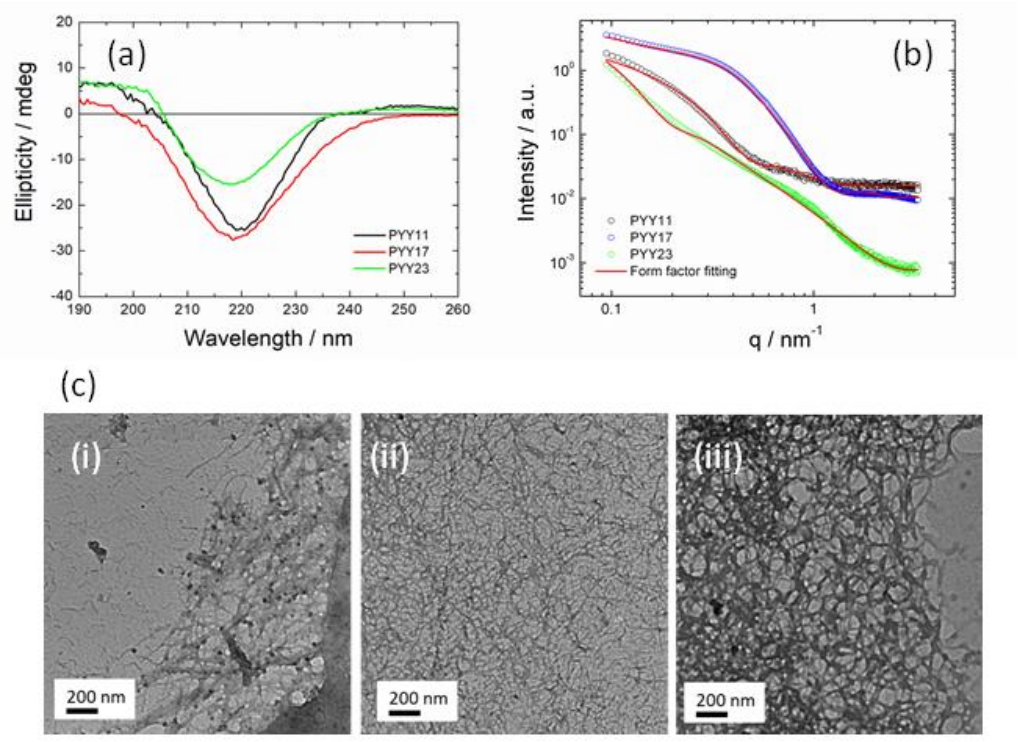


**Figure 8:** (a) CD spectra from gels of all three lipidated peptide at pH 7-8 and 20 °C. (b) SAXS intensity profiles and form factor fittings for gels of PYY11, PYY17, and PYY23 at pH 7-8. All data was fitted to a long cylindrical shell form factor. (c) TEM images of the peptide hydrogels at pH 8. (i) PYY11, (ii) PYY17, (iii) PYY23.

SAXS data measured for the gels is shown in Figure 8b and was fitted to a long cylindrical shell model using SASfit and fitting parameters are shown in Table S6. The scattering pattern and fitting parameters of PYY23 appears to be distinctly different to the other two lipidated peptides. The radius R is significantly larger than the others and the shell thickness DR is significantly lower.

TEM images of all peptide gels (Figure 8c) show a network of entangled fibres, very similar to the cryo-TEM images of the samples in solution. An interesting observation is that PYY11 and PYY23 did not form a gel at pH 2, which is informative in terms of understanding the mechanism of gelation, since they both form micelles at pH 2, whereas PYY17 forms fibres. This indicates that a fibre morphology could be crucial to gelation.

Polarized optical microscopy was carried out on the peptide hydrogels using Congo red as a staining agent to show green birefringence in polarized light from the presence of amyloid fibrils.[64] Birefringence is the result of a sample having two refractive indices and it can change linearly polarized light to elliptically polarized light, to allow light to pass through a crossed analyser.[65] Congo red is an azo dye that has an orientated arrangement on amyloid fibrils by forming hydrogen bonds between amino and hydroxyl groups within the dye and on amyloid structures.[66] When stained with Congo red in alkali conditions, the fibrils appear red in unpolarised light, and green in polarised light. Microscopy images are shown in Figure S27 and yellow/green birefringence is observed for all three lipidated peptides, indicating the presence of amyloid fibrils.

Fibre X-ray diffraction was performed to compliment the SAXS data. The obtained 2D patterns were isotropic, so the data were reduced to one-dimensional form. The resulting intensity profiles are shown in SI Figure S23. The results show $\alpha$-helical structures with sharp peaks corresponding to d spacings = 5.70 Å.

**Conclusions**

Our study provides a comprehensive picture of the influence of palmitoylation and the position of this lipidation on the conformation and self-assembly of the $PYY_{3-36}$ peptide All three lipidated peptides studied exhibit critical aggregation concentrations in pyrene fluorescence probe assays, in the range 0.008 – 0.07 wt%, depending on pH. Pyrene is sensitive to the local hydrophobic environment and so these assays probe "hydrophobic collapse". Comparing samples at a fixed pH, PYY23 and PYY17 have lower cac values than PYY11, this may reflect the replacement of charged arginine residues in these peptides by hydrophobic lipids. The parent peptide $PYY_{3-36}$ itself undergoes a critical aggregation process into fibrils, revealed by Thioflavin T fluorescence assays . The cac values are of the same order of magnitude as those for the lipidated peptides. The cac values increase significantly at low pH.

The lipidated peptides form long entangled fibers above pH 4, but remarkably PYY11 and PYY23 form micelles at low pH. This is in contrast to the non-lipidated peptide which formed a mixture of monomers and twisted nanotapes at pH 2-6, and a mixture of clusters and sheets at pH 8. It is unclear why PYY17 does not form micelles at pH 2, in contrast to PYY11 and PYY23. Cryo-TEM and SAXS clearly indicate the formation of fibrils for this sample under these conditions. PYY11 forms micelles over a wide range of pH values (pH 2 to 6) which presumably due to the fact that this sample is not lipidated in the $\alpha$-helix domain which is therefore unperturbed (and fully charged at lower pH with two unsubstituted arginine residues).

CD results showed an $\alpha$-helical secondary structure throughout a pH range of 2-6 for all peptides, although at pH 8, PYY17 and PYY23 undergo an $\alpha$-helix to $\beta$-sheet transition about 50 $^{o}$ C. The retention of $\alpha$-helical conformation within micelles is unexpected, since lipopeptide micelles observed to date generally comprise peptide groups with disordered conformation due to the constraints imposed by the spherical geometry.

In contrast to the α-helical peptide hydrogel reported by Banwell et al. [61], the PYY lipidated peptide hydrogels are based on β-sheet structure resulting from "denaturation" of the peptide under conditions where the concentration is high enough and the pH is sufficiently large. The α-helix to β-sheet transition was observed for "pre-gel" solutions via CD measurements during high temperature annealing. Although lipidation stabilizes the α-helical conformation against temperature and pH changes compared to the unlipidated $PYY_{3-36}$ peptide, we show that it is possible to destabilize the α-helical conformation ("denaturation" to β-sheet structure") by high temperature annealing. Hydrogelation is observed by pH adjustment at low or high pH. At intermediate pH, gelation is prevented by sample precipitation which occurs at around the presumed pI of the peptides. The PYY lipidated peptide hydrogels may be useful in future formulations of these molecules for therapeutic applications.

In practical terms, Lipidation confers enhanced stability pH and temperature change to a similar extent for all three lipidated peptides, although the absolute value of α-helical content strongly dependent on pH. Unexpectedly, β-sheet structured hydrogels were observed over the widest range of pH values for PYY23, and the lowest range for PYY11. PYY23 is lipidated in the centre of the α-helical domain and this seems to lead to disruption of α-helix structure at the expense of β-sheet conformation at high concentration whereas for PYY11, where the site of lipidation is outside the α-helical domain there is a lower pH range for β-sheet hydrogel formation. Also substitution at S(11) does not change the charge on the peptide, unlike substitution at R(17) or R(23) where there is a net loss of +1 charge (below the pKa of this residue). If hydrogels are required for potential PYY peptide slow release formulations, then our studies suggest that lipidation of the peptide at position 23 provides can be used to produce hydrogels under the widest range of pH conditions. It is hoped that these findings stimulate further research to investigate the influence of lipidation on the conformation and self-assembly of lipidated peptide hormones and that this will benefit future peptide drug development.

**Experimental Section**

**Materials.** Human $PYY_{3-36}$ acetate salt was synthesised by Bachem, Switzerland. The molecular mass by MALDI-MS was measured by the supplier using a Shimadzu Biotech Axima-CFR instrument, and found to be 4049.61 g $mol^{-1}$ (Fig. S1a), (expected: 4047.07 g $mol^{-1}$). The molecular mass was checked in our labs by ESI-MS using a Thermo Scientific LTQ-Orbitrap XL instrument, and found to be 4049.07 g $mol^{-1}$. The purity was 96.9% determined by HPLC using a Dionex Ultimate 3000 HPLC system with Vydac C18 column.

PYY11 acetate salt was custom synthesised by Bachem, Switzerland. The molecular mass by MALDI-MS was measured by the supplier using a Shimadzu Biotech Axima-CFR instrument, and found to be 4458.19 g $mol^{-1}$ (Fig. S1b), (expected: 4454.37 g $mol^{-1}$).The molecular mass was checked in our labs by ESI-MS using a Thermo Scientific LTQ-Orbitrap XL instrument, and found to be 4458.41 g $mol^{-1}$ . The purity was 95.4 % as determined by HPLC using a Dionex Ultimate 3000 HPLC system with Vydac C18 column.

PYY17 acetate salt was custom synthesised by Bachem, Switzerland. The molecular mass by MALDI-MS was measured by the supplier using a Shimadzu Biotech Axima-CFR instrument, and found to be 4389.13 g $mol^{-1}$ (Fig. S1c), (expected: 4387.32 g $mol^{-1}$). The molecular mass was checked in our labs by ESI-MS using a Thermo Scientific LTQ-Orbitrap XL instrument, and found to be 4389.32 g $mol^{-1}$. The purity was 97.8 % as determined by HPLC using a Dionex Ultimate 3000 HPLC system with Vydac C18 column.

PYY23 acetate salt was custom synthesised by Bachem, Switzerland. The molecular mass by MALDI-MS was measured by the supplier using a Shimadzu Biotech Axima-CFR instrument, and found to be 4389.27 g $mol^{-1}$ (Fig. S1d), (expected: 4387.32 g $mol^{-1}$). The molecular mass was checked in our labs by ESI-MS using a Thermo Scientific LTQ-Orbitrap XL instrument, and found to be 4389.33 g $mol^{-}$

[1]. The purity was 98.3% as determined by HPLC using a Dionex Ultimate 3000 HPLC system with Vydac C18 column.

**Fluorescence Spectroscopy.** Fluorescence spectra were recorded with a Varian Cary Eclipse fluorescence spectrometer with samples in 4 mm inner diameter quartz cuvettes. Pyrene assays were performed using 1.3 $x10^{-3}$ to 0.13 wt% peptide solutions, in 2.167 $x10^{-5}$ wt% pyrene solution. The samples were excited at a wavelength $\lambda_{ex}$ = 339 nm, and the fluorescence emission was measured for λ = 360−500 nm.

**Circular Dichroism (CD).** CD spectra were recorded using a Chirascan spectropolarimeter (Applied Photophysics, UK). Spectra are presented with absorbance A < 2 at any measured point with a 0.5 nm step, 1 nm bandwidth, 1 s collection time per step, and 3 repeats. The CD signal from the background (water) was subtracted from the CD signal of the sample solution. Ellipticity is reported as the mean residue ellipticity ([$\theta$], in deg $cm^2$/dmol) and calculated as:

$$[\theta] = [\theta]_{obs} \text{ MRW}/10cl$$

Where $[\theta]_{obs}$ is the ellipticity measured in millidegrees, MRW is the mean residue molecular weight of the peptide (molecular weight divided by the number of amino acid residues), *c* is the concentration of the sample in mg/mL, and *l* is the optical path length of the cell in centimeters.

Samples were measured using quartz plaques (0.2 mm spacing for solutions and 0.01 mm for gels) with 0.5 wt% solution concentrations with a pH range from 2-8. Gel concentrations measured ranged from 1.6-2.4 wt%. CD spectra were measured using a temperature range of 20-70 $^{o}$C and a 5 $^{o}$C step. The sample was equilibrated at each temperature for 2 minutes before measurements were recorded.

**Cryogenic Transmission Electron Microscopy (Cryo-TEM).** Imaging was carried out using a field emission cryo-electron microscope (JEOL JEM-3200FSC) operating at 200 kV. Images were taken using bright-field mode and zero loss energy filtering (omega type) with a slit width of 20 eV.

Micrographs were recorded using a CCD camera (Gatan Ultrascan 4000, USA). The specimen temperature was maintained at -187 $^{o}$C during the imaging. Vitrified specimens were prepared using an automated FEI Vitrobot device using Quantifoil 3.5/1 holey carbon copper grids, with a 3.5 μm hole sizes. Grids were cleaned using a Gatan Solarus 9500 plasma cleaner just prior to use and then transferred into the environmental chamber of a FEI Vitrobot at room temperature and 100% humidity. Following this, 3 μL of sample solution at 0.5 wt % concentration was applied on the grid, blotted once for 1 s, and then vitrified in a 1:1 mixture of liquid ethane and propane at −180 °C. Grids with vitrified sample solutions were maintained in a liquid nitrogen atmosphere and then cryo-transferred into the microscope.

**Polarized Optical Microscopy (POM).** Images were obtained with an Olympus BX41 polarized microscope by placing the sample between crossed polarizers. Approximately 20 μL of Congo red solution (450 μM) was added to gel samples and were left for an hour to allow the Congo red solution to absorb into the gels. The resulting mixtures were placed between a glass slide and a coverslip. Images were collected using an Olympus SP-350 digital camera.

**Small-Angle X-ray Scattering (SAXS).** Solution SAXS experiments were performed on the bioSAXS beamline BM29 at the ESRF, Grenoble, France, and also on the bioSAXS beamline B21 at Diamond, Harwell, UK. Solutions containing 0.5 wt% of peptide in water were loaded into PCR tubes in an automated sample changer. At the ESRF, SAXS data were collected using a Pilatus 1 M detector. The sample−detector distance was 2.84 m. The X-ray wavelength was 0.99 Å. At diamond, SAXS data was collected using a 2 M detector and at a fixed camera length of 3.9 m with a wavelength $\lambda$ = 1 Å. The wavenumber $q = 4\pi \sin\theta / \lambda$ scale was calibrated using silver behenate, where $\lambda$ is the x-ray wavelength and $2\theta$ is the scattering angle. SAXS on hydrogels was performed at Diamond on beamlines I22 and B21. On I22, Samples were placed in DSC pans modified with glass or Teflon windows to enable transmission of the X-ray beam. The sample-to-SAXS detector distance was 7.483 m. A Pilatus P3-2M detector was used to acquire the 2D SAXS scattering patterns. SAXS data

collected for samples with Teflon windows was corrected for the Teflon background scattering. Diffraction from silver behenate was used to calibrate the wavevector scale of the scattering curve. Data processing was performed using software DAWN (Data Analysis Software group, Diamond Light Source Ltd.). On beamline B21 at diamond, samples were placed in custom made gel holder cells with kapton windows. SAXS data was collected using a 2 M detector and at a fixed camera length of 3.9 m with a wavelength $\lambda$ = 1 Å.

**Fiber X-ray Diffraction (XRD).** XRD of gels (1.6-2.4 wt%) was performed on dried peptide stalks prepared by creating a fibre of peptide between the ends of wax coated capillaries. After separation of the capillaries after drying, a stalk was left on the end of one of the capillaries. Stalks were vertically mounted onto the goniometer of an Oxford Diffraction Gemini Ultra instrument, equipped with a Sapphire CCD detector. The sample to detector distance was 44 mm. The X-ray wavelength was $\lambda$ = 1.54 Å. The wavenumber scale ($q = 4\pi \sin\theta/\lambda$ where $2\theta$ is the scattering angle) was geometrically calculated.

**Zeta Potential.** $\zeta$ potentials were measured using a Zetasizer Nano ZS from Malvern Instruments. A 1 mL aliquot of sample was placed inside a disposable folded capillary cell. The sample was left to equilibrate for 120 s before measuring the $\zeta$ potential, using an applied voltage of 50.0 V. The results presented are the average over three measurements.

**pH titration measurement.** pH titrations were carried out using 2 wt% peptide solutions in water (3 mg in 150 µL). Sodium hydroxide (0.25 M) was added to the peptide solutions until pH 10 was reached. Titrations were performed by adding diluted HCl (0.022 M) dropwise, and measuring the pH using a pH meter until the pH had dropped to pH 2. Water was also titrated in the same way as a control experiment.

**Nanodrop Concentration Determination.** For gels, concentrations were measured using a Thermo Scientific NanoDrop 1000 spectrophotometer, and ND-1000 version 3.7 software. 2µL of each

sample was pipetted onto a cleaned measurement pedestal. The absorbance at 280nm was recorded. A molar absorbance coefficient was calculated using the following equation,ε = (nW × 5500) + (nY × 1490) + (nC × 125). At 280 nm, this is the weighted sum of the 280 nm molar absorption coefficients of tryptophan (W), tyrosine (Y) and cysteine (C) amino acids. Given there are four tyrosine residues in each of the lipidated peptides this equation produces a molar absorbance coefficient of 5960 L $mol^{-1}$ $cm^{-1}$. This absorbance and molar absorbance coefficient were then used to calculate the molarity using the Beer-Lambert equation. From the molarity the weight of peptide present was found and subsequently converted to a weight percent, using known volumes and molecular weights.

**Preparation of Hydrogels.** Gels were prepared by making up 1-2 wt% peptide solutions in ultrapure water (18 MΩ Barnstead Nanopure, ThermoScientific, USA), and changing the pH accordingly using 1M HCl or 1M NaOH. The solutions were heated to 60 $^{o}$C for approximately 2-10 hours and then left to stand for a couple of hours to a couple of days for the gelation to occur. The concentration of gels were determined by Nanodrop experiments and ranged from 1.6-2.4 wt% .The pH range studied was pH 2-8.

**Transmission electron microscopy (TEM).** Imaging was performed using a JEOL AMT. XR-401 TEM instrument. A thin film of peptide gel was added to the surface of a carbon film coated TEM grid and stained with 1 wt% uranyl acetate solution for 1 minute, followed by washing with distilled water by applying enough water to cover the grid and leaving it for 1 minute. The grids were then taken and placed in the TEM Instrument and images were taken, using a 4.0 megapixel CMOS camera, at various magnifications.

**Acknowledgements**

We thank Medimmune and the University of Reading for co-funding postgraduate studentships for JH and SB. We thank Shahid Uddin, Steve Bishop and Ramesh Shanmugam at Medimmune for stimulating discussions. We are grateful to the ESRF for the award of beamtime (MX-1869) on

beamline BM29 and Martha Brennich for assistance. We thank Diamond for the award of beamtime on beamline B21 and Nathan Cowieson, Katsuaki Inoue and Rob Rambo for valuable help. We thank Peter Harris at the Electron Microscopy lab (University of Reading) for assistance with TEM. Use of facilities of the Chemical Analysis Facility (CAF) at the University of Reading is also acknowledged.

**Supporting Information**

The Supporting Information is available free of charge on the ACS Publications website at DOI: XX.XXXX/acsami.XXXXXXX

Tables of zeta potential values and SAXS fit parameters, MALDI-MS spectra, titration curves, additional cac data, cryo-TEM images, SAXS data with fits, images of gels, fibre XRD profiles and polarized optical microscopy images.

**References**


1. Henry, K. E.; Elfers, C. T.; Burke, R. M.; Chepurny, O. G.; Holz, G. G.; Blevins, J. E.; Roth, C. L.; Doyle, R. P., Vitamin B12 Conjugation of Peptide-YY3–36 Decreases Food Intake Compared to Native Peptide-YY3–36 Upon Subcutaneous Administration in Male Rats. *Endocrinology* **2015,** *156* (5), 1739-1749.
2. http://rzlab.ucr.edm/scripts/wheel/wheel.cgi. Accessed in 2018.
3. Nygaard, R.; Nielbo, S.; Schwartz, T. W.; Poulsen, F. M., The PP-Fold Solution Structure of Human Polypeptide YY and Human $PYY_{3-36}$ as Determined by NMR. *Biochem.* **2006,** *45* (27), 8350-7.
4. Keire, D. A.; Mannon, P.; Kobayashi, M.; Walsh, J. H.; Solomon, T. E.; Reeve, J. R., Primary Structures of PYY, [Pro(34)]PYY, and PYY-(3-36) Confer Different Conformations and Receptor Selectivity. *Am. J. Physiol. Gastrointest. Liver. Physiol.* **2000,** *279* (1), G126-G131.
5. Hutchinson, J. A.; Burholt, S.; Hamley, I. W., Peptide Hormones and Lipopeptides: From Self-Assembly to Therapeutic Applications. *J. Pept. Sci.* **2017,** *23*, 82-94.
6. Wren, A. M.; Bloom, S. R., Gut Hormones and Appetite Control. *Gastroenterology* **2007,** *132* (6), 2116-2130.
7. De Silva, A.; Bloom, S. R., Gut Hormones and Appetite Control: A Focus on PYY and GLP-1 as Therapeutic Targets in Obesity. *Gut Liver* **2012,** *6* (1), 10-20.
8. Strader, A. D.; Woods, S. C., Gastrointestinal Hormones and Food Intake. *Gastroenterology* **2005,** *128* (1), 175-191.
9. Yu, Y. C.; Berndt, P.; Tirrell, M.; Fields, G. B., Self-Assembling Amphiphiles for Construction of Protein Molecular Architecture. *J. Am. Chem. Soc.* **1996,** *118* (50), 12515-12520.
10. Zhang, L.; Bulaj, G., Converting Peptides into Drug Leads by Lipidation. *Curr. Med. Chem.* **2012,** *19* (11), 1602-1618.
11. Bellmann-Sickert, K.; Elling, C. E.; Madsen, A. N.; Little, P. B.; Lundgren, K.; Gerlach, L. O.; Bergmann, R.; Holst, B.; Schwartz, T. W.; Beck-Sickinger, A. G., Long-Acting Lipidated Analogue

of Human Pancreatic Polypeptide Is Slowly Released into Circulation. *J. Med. Chem.* **2011,** *54* (8), 2658-2667.

12. Simerska, P.; Moyle, P. M.; Toth, I., Modern Lipid-, Carbohydrate-, and Peptide-Based Delivery Systems for Peptide, Vaccine, and Gene Products. *Med. Res. Rev.* **2011,** *31* (4), 520-547.
13. Tatemoto, K., Isolation and Characterization of Peptide YY (PYY), a Candidate Gut Hormone That Inhibits Pancreatic Exocrine Secretion. *Proc. Nat. Acad. Sci. USA* **1982,** *79* (8), 2514-2518.
14. Madsen, K.; Knudsen, L. B.; Agersoe, H.; Nielsen, P. F.; Thogersen, H.; Wilken, M.; Johansen, N. L., Structure-Activity and Protraction Relationship of Long-Acting Glucagon-Like Peptide-1 Derivatives: Importance of Fatty Acid Length, Polarity, and Bulkiness. *J. Med Chem* **2007,** *50* (24), 6126-32.
15. Keire, D. A.; Kobayashi, M.; Solomon, T. E.; Reeve, J. R., Solution Structure of Monomeric Peptide YY Supports the Functional Significance of the PP-Fold. *Biochemistry* **2000,** *39* (32), 9935-9942.
16. Fuhlendorff, J.; Johansen, N. L.; Melberg, S. G.; Thogersen, H.; Schwartz, T. W., The Antiparallel Pancreatic-Polypeptide Fold in the Binding of Neuropeptide-Y to Y1-Receptors and Y2-Receptors. *J. Biol. Chem.* **1990,** *265* (20), 11706-11712.
17. Parker, S. L.; Balasubramaniam, A., Neuropeptide Y Y2 receptor in health and disease (vol 153, pg 420, 2007). *Br. J. Pharmacol* **2008,** *155* (8), 1307-1307.
18. Ballantyne, G. H., Peptide YY(1-36) and Peptide YY(3-36): Part I. Distribution, Release and Actions. *Obes. Surg.* **2006,** *16* (5), 651-658.
19. Batterham, R. L.; Bloom, S. R., The Gut Hormone Peptide YY Regulates Appetite. *Ann. N.Y. Acad. Sci.* **2003,** *994*, 162-168.
20. Chamorro, S.; Della-Zuana, O.; Fauchere, J. L.; Feletou, M.; Galizzi, J. P.; Levens, N., Appetite Suppression Based on Selective Inhibition of NPY Receptors. *Int. J. Obes. Relat. Metab. Disord.* **2002,** *26* (3), 281-98.

21. Ehrlich, G. K.; Michel, H.; Truitt, T.; Riboulet, W.; Pop-Damkov, P.; Goelzer, P.; Hainzl, D.; Qureshi, F.; Lueckel, B.; Danho, W.; Conde-Knape, K.; Konkar, A., Preparation and Characterization of Albumin Conjugates of a Truncated Peptide YY Analogue for Half-Life Extension. *Bioconjugate Chem.* **2013,** *24* (12), 2015-2024.

22. Keire, D. A.; Bowers, C. W.; Solomon, T. E.; Reeve, J. R., Structure and Receptor Binding of PYY Analogs. *Peptides* **2002,** *23* (2), 305-321.

23. Albertsen, L.; Andersen, J. J.; Paulsson, J. F.; Thomsen, J. K.; Norrild, J. C.; Stromgaard, K., Design and Synthesis of Peptide YY Analogues with C-terminal Backbone Amide-to-Ester Modifications. *ACS Med. Chem. Lett.* **2013,** *4* (12), 1228-1232.

24. Tang, L.; Persky, A. M.; Hochhaus, G.; Meibohm, B., Pharmacokinetic Aspects of Biotechnology Products. *J. Pharm. Sci.* **2004,** *93*, 2184-2204.

25. Tryggvason, K.; Wartiovaara, J., How Does the Kidney Filter Plasma? *Physiology* **2005,** *20*, 96-101.

26. Bellmann-Sickert, K.; Beck-Sickinger, A. G., Peptide Drugs to Target G Protein-Coupled Receptors. *Trends. Pharmacol. Sci.* **2010,** *31* (9), 434-441.

27. Knop, K.; Hoogenboom, R.; Fischer, D.; Schubert, U. S., Poly(Ethylene Glycol) in Drug Delivery: Pros and Cons as Well as Potential Alternatives. *Angew. Chem. Int. Ed. Engl.* **2010,** *49* (36), 6288-6308.

28. Harris, J. M.; Chess, R. B., Effect of PEGylation on Pharmaceuticals. *Nat. Rev. Drug. Disc.* **2003,** *2*, 214-221.

29. Knudsen, L. B.; Nielsen, P. F.; Huusfeldt, P. O.; Johansen, N. L.; Madsen, K.; Pedersen, F. Z.; Thogersen, H.; Wilken, M.; Agerso, H., Potent Derivatives of Glucagon-Like-Peptide-1 with Pharmacokinetic Properties Suitable for Once Daily Administration. *J. Med. Chem.* **2000,** *43*, 1664-1669.

30. Pan, C. Q.; Buxton, J. M.; Yung, S. L.; Tom, I.; Yang, L.; Chen, H.; MacDougall, M.; Bell, A.; Claus, T. H.; Clairmont, K. B.; Whelan, J. P., Design of a Long Acting Peptide Functioning as Both a

Glucagon-like Peptide-1 Receptor Agonist and a Glucagon Receptor Antagonist. *J. Biol. Chem.* **2006,** *281* (18), 12506-12515.

31. Thorens, B., Expression Cloning of the Pancreatic B cell Receptor for the Gluco-Incretin Hormone Glucagon-Like Peptide-1. *Proc. Natl. Acad. Sci.* **1992,** *89*, 8641-8645.

32. Thieme, V.; Jolly, N.; Madsen, A. N.; Bellmann-Sickert, K.; Schwartz, T. W.; Holst, B.; Cox, H. M.; Beck-Sickinger, A. G., High Molecular Weight PEGylation of Human Pancreatic Polypeptide at Position 22 Improves Stability and Reduces Food Intake in Mice. *Br. J. Pharmacol* **2016,** *173* (22), 3208-3221.

33. Kalyanasundaram, K.; Thomas, J. K., Environmental Effects on Vibronic Band Intensities in Pyrene Monomer Fluorescence and their Application in Studies of Micellar Systems. *J. Am. Chem. Soc.* **1977,** *99* (7), 2039-2044.

34. Hamley, I. W.; Dehsorkhi, A.; Castelletto, V.; Walter, M. N. M.; Connon, C. J.; Reza, M.; Ruokolainen, J., Self-Assembly and Collagen-Stimulating Activity of a Peptide Amphiphile Incorporating a Peptide Sequence from Lumican. *Langmuir* **2015,** *31* (15), 4490-4495.

35. Miravet, J. F.; Escuder, B.; Segarra-Maset, M. D.; Tena-Solsona, M.; Hamley, I. W.; Dehsorkhi, A.; Castelletto, V., Self-Assembly of a Peptide Amphiphile: Transition from Nanotape Fibrils to Micelles. *Soft Matter* **2013,** *9* (13), 3558-3564.

36. Castelletto, V.; Gouveia, R. M.; Connon, C. J.; Hamley, I. W.; Seitsonen, J.; Nykanen, A.; Ruokolainen, J., Alanine-Rich Amphiphilic Peptide Containing the RGD Cell Adhesion Motif: A Coating Material for Human Fibroblast Attachment and Culture. *Biomater. Sci.* **2014,** *2* (3), 362-369.

37. Urry, D. W.; Peng, S. Q.; Parker, T. M.; Gowda, D. C.; Harris, R. D., Relative Significance of Electrostatic- and Hydrophobic-Induced pKa Shifts in a Model Protein: The Aspartic Acid Residue. *Angew. Chem. Int. Ed. Engl.* **1993,** *32* (10), 1440-1442.

38. Isom, D. G.; Castaneda, C. A.; Cannon, B. R.; Garcia-Moreno, B., Large Shifts in pKa Values of Lysine Residues Buried Inside a Protein. *Proc. Nat. Acad. Sci. U S A* **2011,** *108* (13), 5260-5.

39. Tang, C.; Smith, A. M.; Collins, R. F.; Ulijn, R. V.; Saiani, A., Fmoc-Diphenylalanine Self-Assembly Mechanism Induces Apparent pKa Shifts. *Langmuir* **2009,** *25* (16), 9447-53.

40. Woody, R. W., Circular Dichroism of Peptides and Proteins. In *Circular Dichroism: Principles and Applications*, Berova, N., Nakanishi, K. and Woody, R.W., Eds., Wiley: New York, 2000; pp 473-496.

41. Bulheller, B. M.; Rodger, A.; Hirst, J. D., Circular and Linear Dichroism of Proteins. *Phys Chem Chem Phys* **2007,** *9* (17), 2020-2035.

42. Norden, B.; Rodger, A.; Dafforn, T., Linear Dichroism and Circular Dichroism: *Linear Dichroism and Circular Dichroism: A Textbook on Polarized Light Spectroscopy* RSC: Cambridge, UK, 2010.

43. Su, J. Y.; Hodges, R. S.; Kay, C. M., Effect of Chain Length on the Formation and Stability of Synthetic $\alpha$-Helical Coiled Coils. *Biochem.* **1994,** *33*, 15501-15510.

44. Vandermeulen, G. W. M.; Tziatzios, C.; Klok, H.-A., Reversible Self-Organization of Poly(ethylene glycol)-Based Hybrid Block Copolymers Mediated by a De Novo Four-Stranded α-Helical Coiled Coil Motif. *Macromolecules* **2003,** *36* (11), 4107-4114.

45. Cerpa, R.; Cohen, F. E.; Kuntz, I. D., Conformational Switching in Designed Peptides: The Helix/Sheet Transition. *Folding and Design* **1996,** *1* (2), 91-101.

46. da Silva, E. R.; Walter, M. N. M.; Reza, M.; Castelletto, V.; Ruokolainen, J.; Connon, C. J.; Alves, W. A.; Hamley, I. W., Self-Assembled Arginine-Capped Peptide Bolaamphiphile Nanosheets for Cell Culture and Controlled Wettability Surfaces. *Biomacromolecules* **2015,** *16* (10), 3180-3190.

47. Dehsorkhi, A.; Castelletto, V.; Hamley, I. W.; Adamcik, J.; Mezzenga, R., The Effect of pH on the Self-Assembly of a Collagen Derived Peptide Amphiphile. *Soft Matter* **2013,** *9* (26), 6033-6036.

48. Hamley, I. W.; Hutchinson, J.; Kirkham, S.; Castelletto, V.; Kaur, A.; Reza, M.; Ruokolainen, J., Nanosheet Formation by an Anionic Surfactant-Like Peptide and Modulation of Self-Assembly through Ionic Complexation. *Langmuir* **2016,** *32* (40), 10387-10393.

49. Bressler, I.; Kohlbrecher, J.; Thünemann, A. F., SASfit: A Tool for Small-Angle Scattering Data Analysis using a Library of Analytical Expressions. *J. Appl. Crystallogr.* **2015,** *48*, 1587-1598.

50. Hartgerink, J. D.; Beniash, E.; Stupp, S. I., Peptide-amphiphile nanofibers: A versatile scaffold for the preparation of self-assembling materials. *Proc. Nat. Acad. Sci.USA* **2002,** *99* (8), 5133-5138.

51. Paramonov, S. E.; Jun, H. W.; Hartgerink, J. D., Self-assembly of peptide-amphiphile nanofibers: The roles of hydrogen bonding and amphiphilic packing. *J. Am. Chem. Soc.* **2006,** *128* (22), 7291-7298.

52. Stendahl, J. C.; Rao, M. S.; Guler, M. O.; Stupp, S. I., Intermolecular forces in the self-assembly of peptide amphiphile nanofibers. *Adv. Funct. Mater.* **2006,** *16* (4), 499-508.

53. Castelletto, V.; Cheng, G.; Stain, C.; Connon, C. J.; Hamley, I. W., Self-Assembly of a Peptide Amphiphile Containing L-Carnosine and Its Mixtures with a Multilamellar Vesicle Forming Lipid. *Langmuir* **2012,** *28* (31), 11599-11608.

54. Pashuck, E. T.; Cui, H. G.; Stupp, S. I., Tuning Supramolecular Rigidity of Peptide Fibers through Molecular Structure. *J. Am. Chem. Soc.* **2010,** *132* (17), 6041-6046.

55. Rexeisen, E. L.; Fan, W.; Pangburn, T. O.; Taribagil, R. R.; Bates, F. S.; Lodge, T. P.; Tsapatsis, M.; Kokkoli, E., Self-Assembly of Fibronectin Mimetic Peptide-Amphiphile Nanofibers. *Langmuir* **2010,** *26* (3), 1953-1959.

56. Rodriguez, L. M. D.; Hemar, Y.; Cornish, J.; Brimble, M. A., Structure-mechanical property correlations of hydrogel forming beta-sheet peptides. *Chem. Soc. Rev.* **2016,** *45* (17), 4797-4824.

57. Hosseinkhani, H.; Hosseinkhani, M.; Khademhosseini, A.; Kobayashi, H.; Tabata, Y., Enhanced angiogenesis through controlled release of basic fibroblast growth factor from peptide amphiphile for tissue regeneration. *Biomaterials* **2006,** *27* (34), 5836-5844.

58. Anderson, J. M.; Andukuri, A.; Lim, D. J.; Jun, H. W., Modulating the Gelation Properties of Self-Assembling Peptide Amphiphiles. *Acs Nano* **2009,** *3* (11), 3447-3454.

59. Kim, J. K.; Anderson, J.; Jun, H. W.; Repka, M. A.; Jo, S., Self-Assembling Peptide Amphiphile-Based Nanofiber Gel for Bioresponsive Cisplatin Delivery. *Mol. Pharm.* **2009,** *6* (3), 978-985.

60. Castelletto, V.; Kaur, A.; Hamley, I. W.; Barnes, R. H.; Karatzas, K. A.; Hermida-Merino, D.; Swioklo, S.; Connon, C. J.; Stasiak, J.; Reza, M.; Ruokolainen, J., Hybrid membrane biomaterials from self-assembly in polysaccharide and peptide amphiphile mixtures: controllable structural and mechanical properties and antimicrobial activity. *RSC Adv* **2017,** *7* (14), 8366-8375.

61. Banwell, E. F.; Abelardo, E. S.; Adams, D. J.; Birchall, M. A.; Corrigan, A.; Donald, A. M.; Kirkland, M.; Serpell, L. C.; Butler, M. F.; Woolfson, D. N., Rational design and application of responsive alpha-helical peptide hydrogels. *Nat. Mater* .**2009,** *8* (7), 596-600.

62. Tang, C.; Ulijn, R. V.; Saiani, A., Effect of Glycine Substitution on Fmoc-Diphenylalanine Self-Assembly and Gelation Properties. *Langmuir* **2011,** *27* (23), 14438-14449.

63. Adams, D. J.; Mullen, L. M.; Berta, M.; Chen, L.; Frith, W. J., Relationship Between Molecular Structure, Gelation Behaviour and Gel Properties of Fmoc-Dipeptides. *Soft Matter* **2010,** *6* (9), 1971-1980.

64. Hamley, I. W., Peptide fibrillization. *Angew. Chem. Int. Ed. Engl.***2007,** *46* (43), 8128-8147.

65. Howie, A. J.; Brewer, D. B.; Howell, D.; Jones, A. P., Physical basis of colors seen in Congo red-stained amyloid in polarized light. *Lab. Invest.* **2008,** *88* (3), 232-242.

66. Howie, A. J.; Brewer, D. B., Optical properties of amyloid stained by Congo red: History and mechanisms. *Micron* **2009,** *40* (3), 285-301.

**Table of Contents Entry**